Electronic Supplementary Information

Adducts of a Sterically Hindered Tellurium(IV) Catecholate with Diimines

Pavel A. Petrov,[a]* Elizaveta A. Filippova,[a] Taisiya S. Sukhikh,[a] Dmitriy G. Sheven,[a] and Alexander S. Novikov[b,c]

[a] Nikolaev Institute of Inorganic Chemistry SB RAS, Prosp. Lavrentieva 3, 630090 Novosibirsk, Russia; e-mail: panah@niic.nsc.ru

[b] Institute of Chemistry, Saint Petersburg State University, Universitetskaya Nab., 7/9, 199034 Saint Petersburg, Russia;

[c] Peoples' Friendship University of Russia (RUDN University), Miklukho-Maklaya Street, 6, Moscow, 117198, Russia.

Contents

Table S1. Crystal data and structure refinement for structures **1**, **3**·C_7H_8, **4**·0.5CH_2Cl_2, **5**·C_7H_8, **6** and **7**.

Identification code	**1**	**3**·C_7H_8	**4**·0.5CH_2Cl_2	**5**·C_7H_8	**6**	**7**
Empirical formula	$C_{28}H_{40}O_4Te$	$C_{87}H_{104}N_4O_8Te_2$	$C_{80.5}H_{97}O_{10}N_4Te_2Cl$	$C_{91}H_{112}N_4O_8Te_2$	$C_{48}H_{64}O_4N_2Te$	$C_{64}H_{86}N_4O_8Te_2$
Formula weight	568.20	1588.94	1571.27	1645.04	860.61	1294.56
Crystal system, space group	Triclinic, P-1	Triclinic, P-1	Monoclinic, $P2_1/c$	Triclinic, P-1	Monoclinic, C2/c	Triclinic, P-1
a/Å	10.7879(19)	10.5866(11)	11.6110(3)	10.0622(2)	15.5230(3)	10.2838(3)
b/Å	11.946(2)	13.8449(13)	18.3720(7)	18.5721(5)	20.9039(5)	11.0436(3)
c/Å	21.895(4)	15.3756(15)	18.9824(8)	22.3625(6)	13.8186(4)	14.4322(4)
α/°	80.413(6)	107.420(4)	90	80.2200(10)	90	71.0190(10)
β/°	79.028(5)	108.898(3)	106.9460(10)	86.4680(10)	95.5510(10)	85.0980(10)
γ/°	75.662(5)	98.439(4)	90	84.5760(10)	90	82.0150(10)
Volume/$Å^3$	2662.5(9)	1958.8(3)	3873.5(2)	4095.43(18)	4462.99(19)	1533.50(8)
Z	4	1	2	2	4	1
ρ_{calc}/g cm^{-3}	1.417	1.347	1.347	1.334	1.281	1.402
μ/mm^{-1}	1.147	0.803	0.846	0.770	0.710	1.007
F(000)	1168.0	822.0	1618.0	1708.0	1800.0	666.0
Crystal size/mm	0.28×0.03×0.03	0.13×0.11×0.09	0.18×0.10×0.09	0.2×0.11×0.07	0.23×0.1×0.08	0.11×0.05×0.05
2Θ range for data collection/°	3.548–50.076	4.56–59.216	4.312–52.76	4.07–54.206	4.244–54.22	4.892–54.292
Index ranges	$-12 \le h \le 12$, $-14 \le k \le 14$, $-26 \le l \le 26$	$-14 \le h \le 14$, $-18 \le k \le 19$, $-20 \le l \le 21$	$-14 \le h \le 14$, $-22 \le k \le 21$, $-16 \le l \le 23$	$-12 \le h \le 12$, $-23 \le k \le 23$, $-28 \le l \le 28$	$-19 \le h \le 19$, $-26 \le k \le 26$, $-17 \le l \le 17$	$-13 \le h \le 13$, $-14 \le k \le 14$, $-18 \le l \le 18$
Reflections collected (R_{int})	16229 (0.0990)	39449 (0.0522)	22103 (0.0478)	56055 (0.0461)	23856 (0.0442)	17075 (0.0459)
Data/restraints/parameters	9281/0/619	10687/61/464	7878/0/445	17956/223/1016	4926/0/258	6761/0/364
Goodness-of-fit on F^2	0.933	1.042	1.025	0.995	1.010	0.965
Final R indexes [I>=2σ(I)]	R_1 = 0.0723, wR_2 = 0.1504	R_1 = 0.0343, wR_2 = 0.0751	R_1 = 0.0356, wR_2 = 0.0707	R_1 = 0.0376, wR_2 = 0.0852	R_1 = 0.0240, wR_2 = 0.0559	R_1 = 0.0417, wR_2 = 0.0962
Final R indexes [all data]	R_1 = 0.1366, wR_2 = 0.1762	R_1 = 0.0405, wR_2 = 0.0791	R_1 = 0.0564, wR_2 = 0.0766	R_1 = 0.0590, wR_2 = 0.0938	R_1 = 0.0305, wR_2 = 0.0579	R_1 = 0.0522, wR_2 = 0.1062
Largest diff. peak/hole/e $Å^{-3}$	1.64/–1.42	1.03/–0.87	0.42/–0.49	0.66/–0.54	0.37/–0.39	1.64/–0.73
CCDC	2287464	2287467	2287466	2287465	2287463	2287462

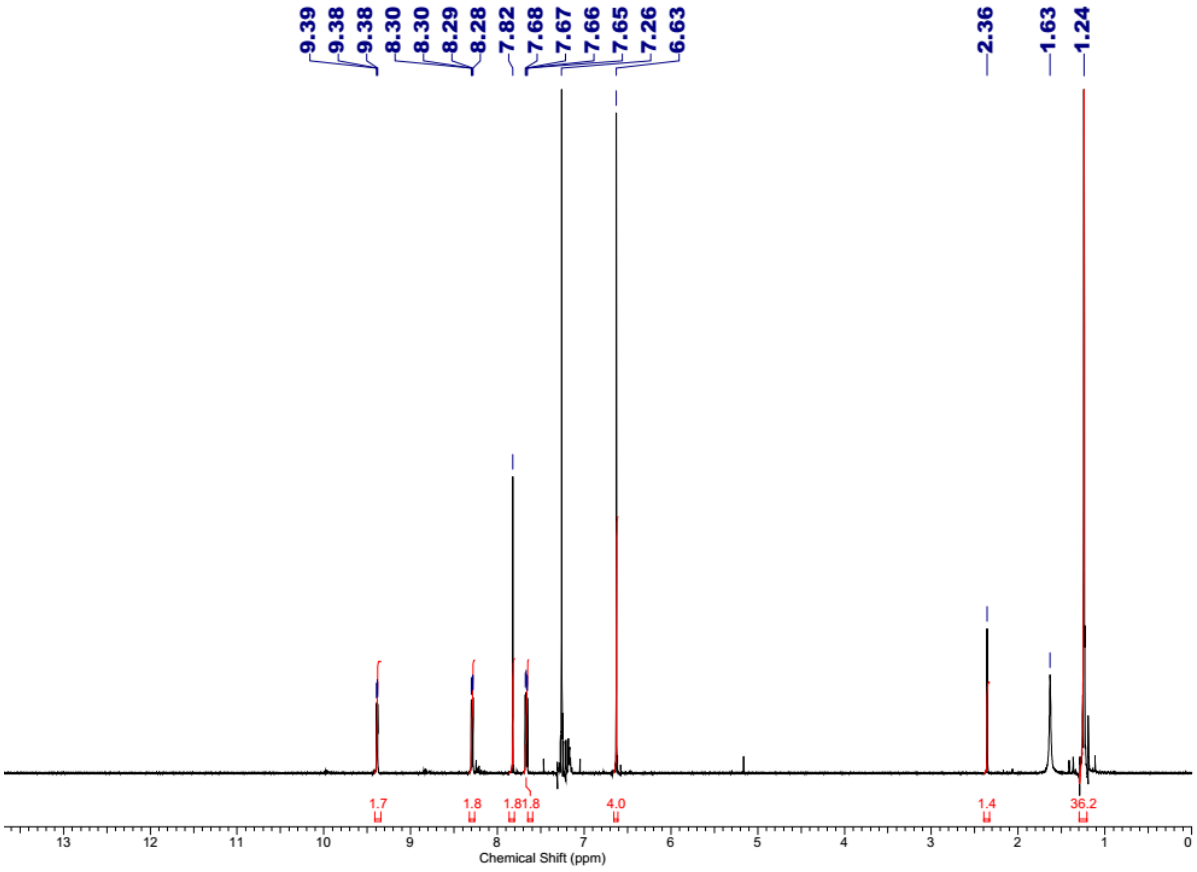

Fig. S1. ^{1}H NMR spectrum of $[Te(Cat^{36})_2(phen)]_2 \cdot C_7H_8$ (**3**$\cdot C_7H_8$) ($CDCl_3$, 298K).

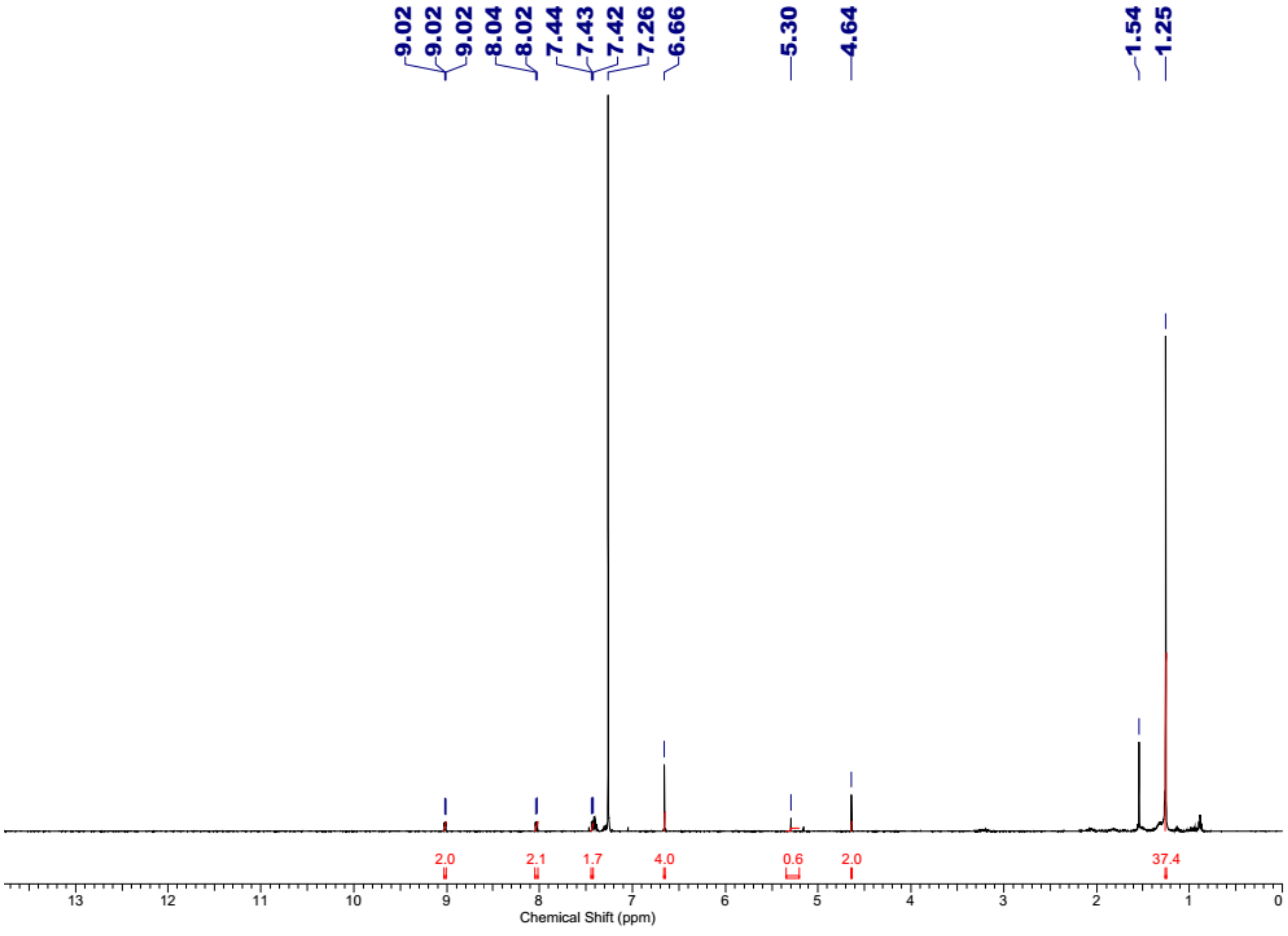

Fig. S2. ^{1}H NMR spectrum of $[Te(Cat^{36})_2(phenO)]_2 \cdot 0.5CH_2Cl_2$ (**4**$\cdot 0.5CH_2Cl_2$) ($CDCl_3$, 298K).

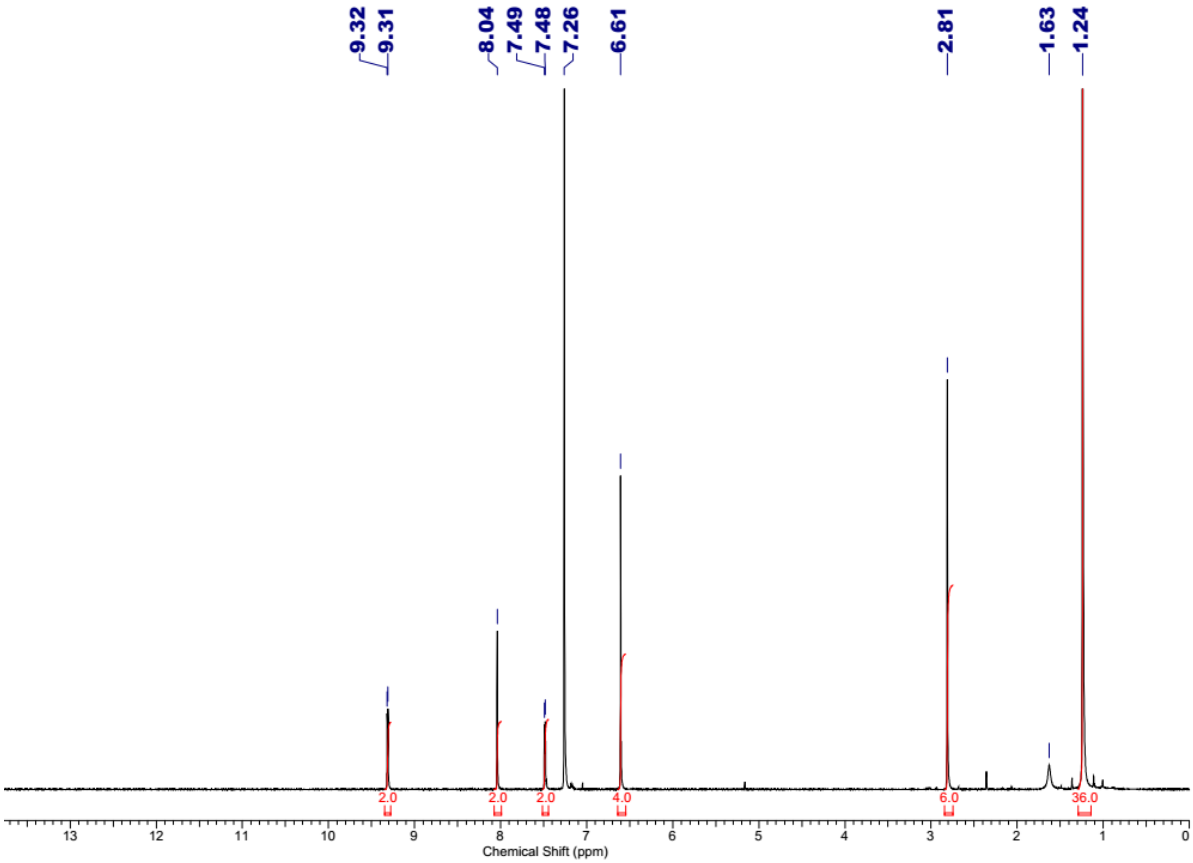

Fig. S3. ^{1}H NMR spectrum of [Te(Cat^{36})$_2$(phenMe$_2$)]$_2$ (**5**) ($CDCl_3$, 298K).

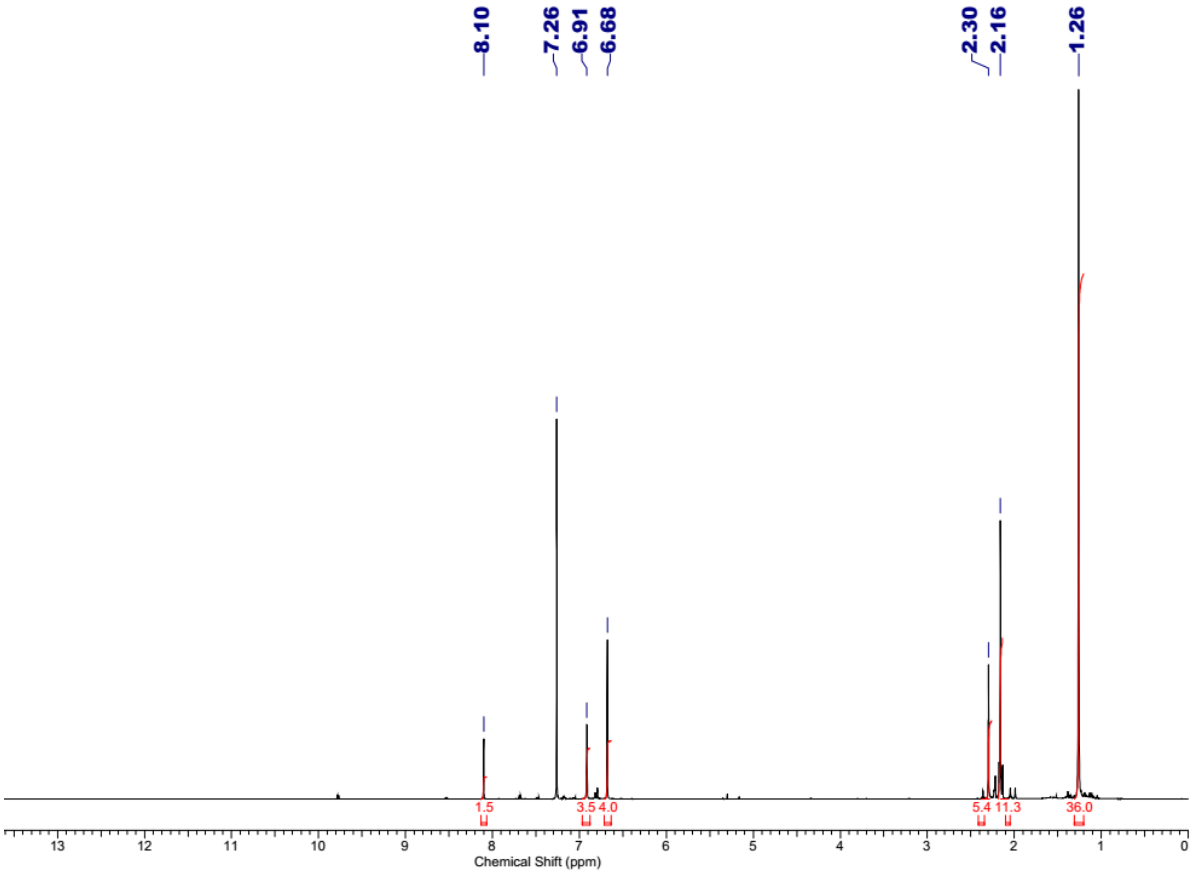

Fig. S4. ^{1}H NMR spectrum of [Te(Cat^{36})$_2$(DAB^{Mes,H})]$_\infty$ (**6**) ($CDCl_3$, 298K).

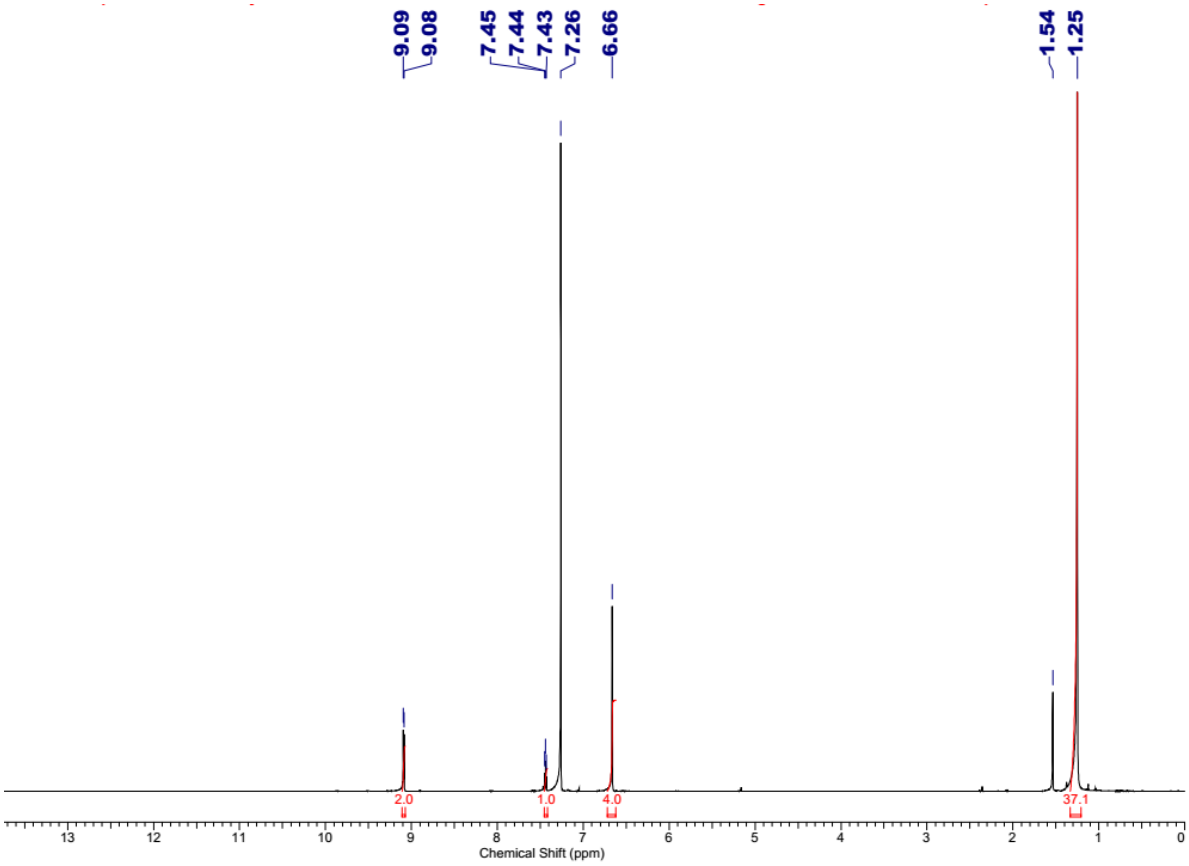

Fig. S5. ^{1}H NMR spectrum of [{Te(Cat^{36})$_2$}$_2$(bpm)] (**7**) ($CDCl_3$, 298K).

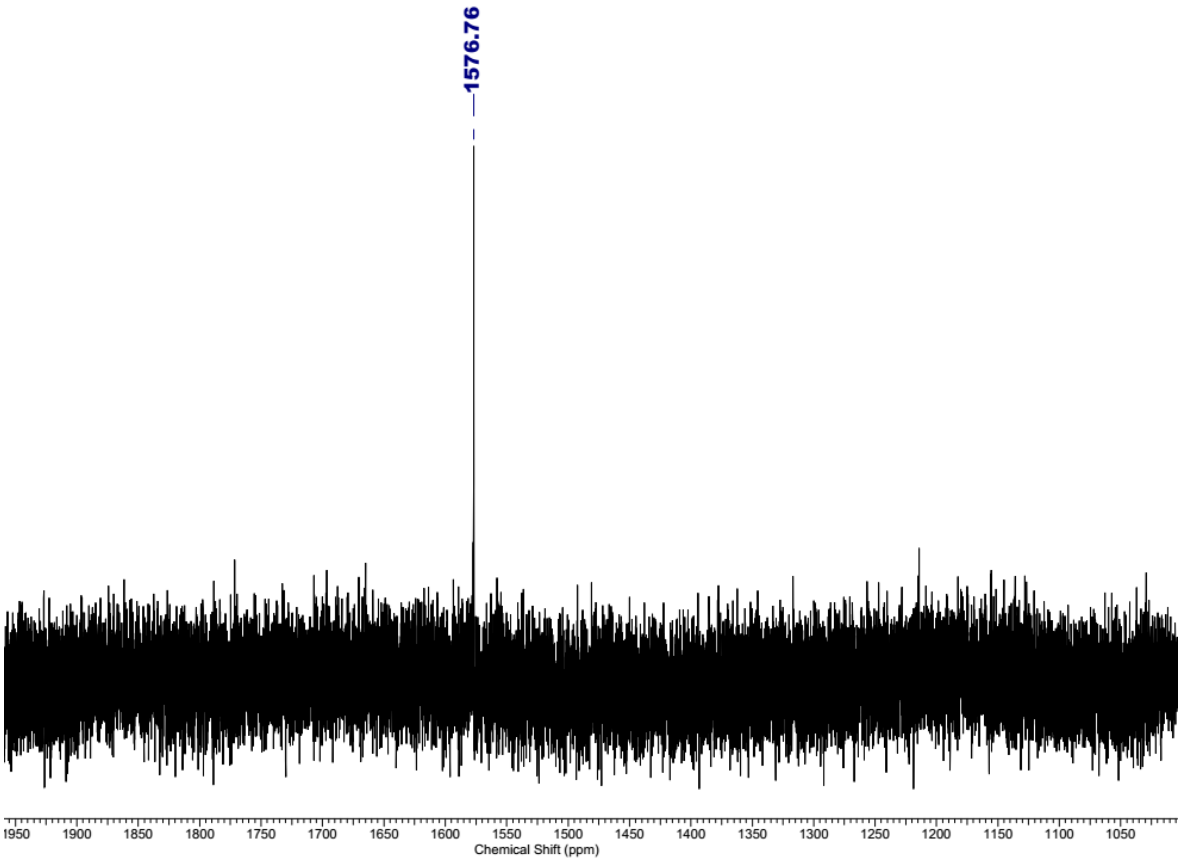

Fig. S6. ^{125}Te NMR spectrum of [Te(Cat^{36})$_2$(phen)]$_2$·C_7H_8 (**3**·C_7H_8) (CH_2Cl_2, 298K).

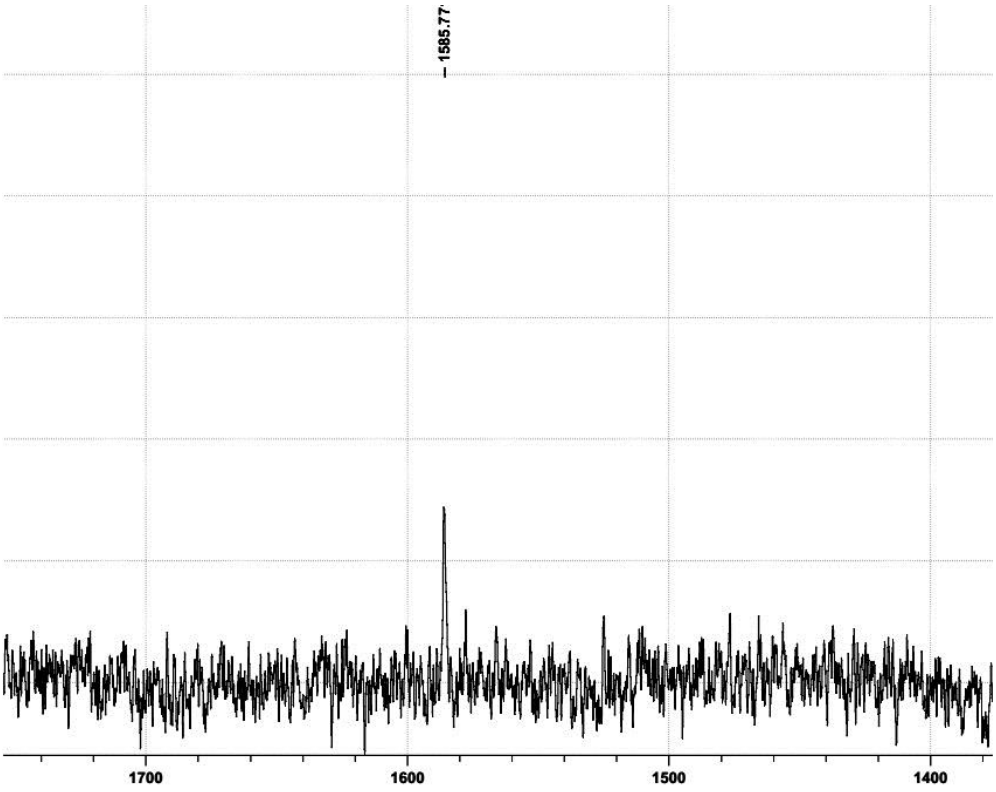

Fig. S7. ^{125}Te NMR spectrum of $[Te(Cat^{36})_2(phenO)]_2 \cdot 0.5CH_2Cl_2$ (**4**$\cdot 0.5CH_2Cl_2$) (CH_2Cl_2, 298K).

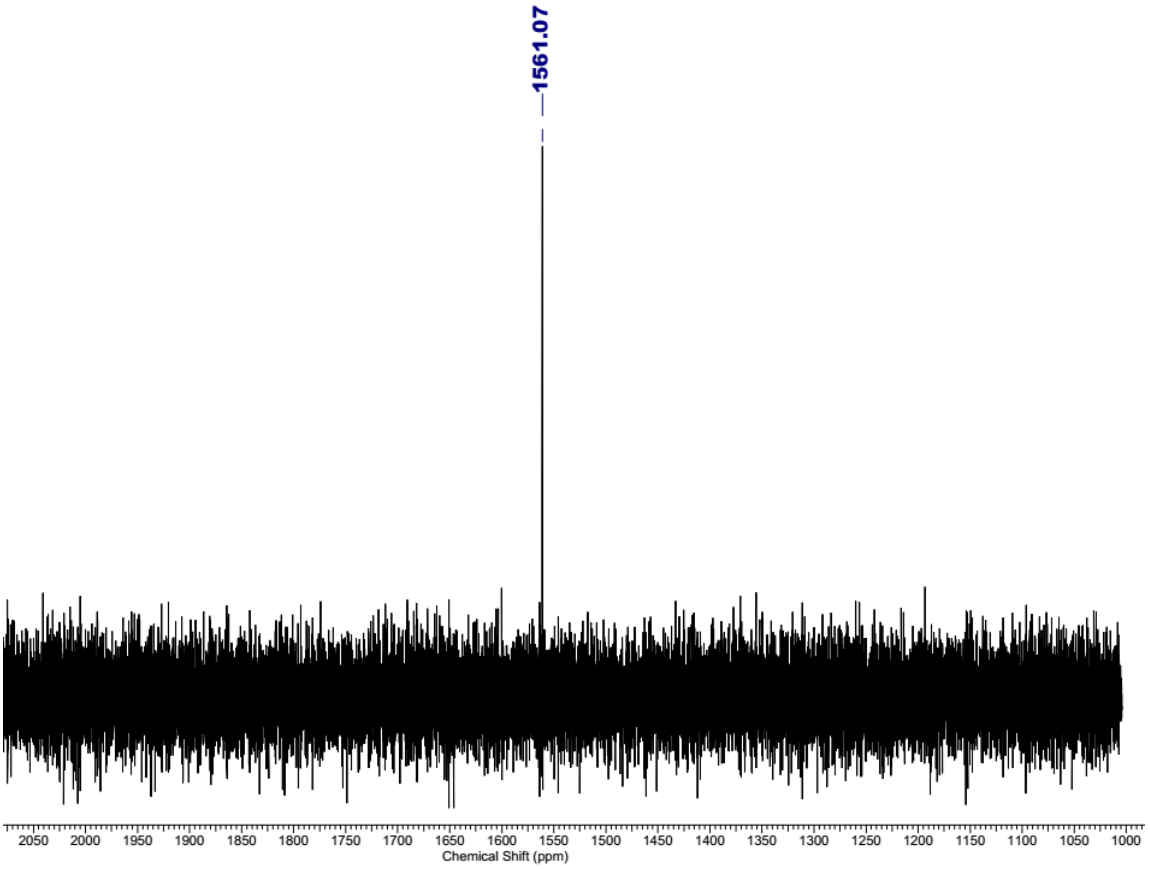

Fig. S8. ^{125}Te NMR spectrum of $[Te(Cat^{36})_2(phenMe_2)]_2$ (**5**) (CH_2Cl_2, 298K).

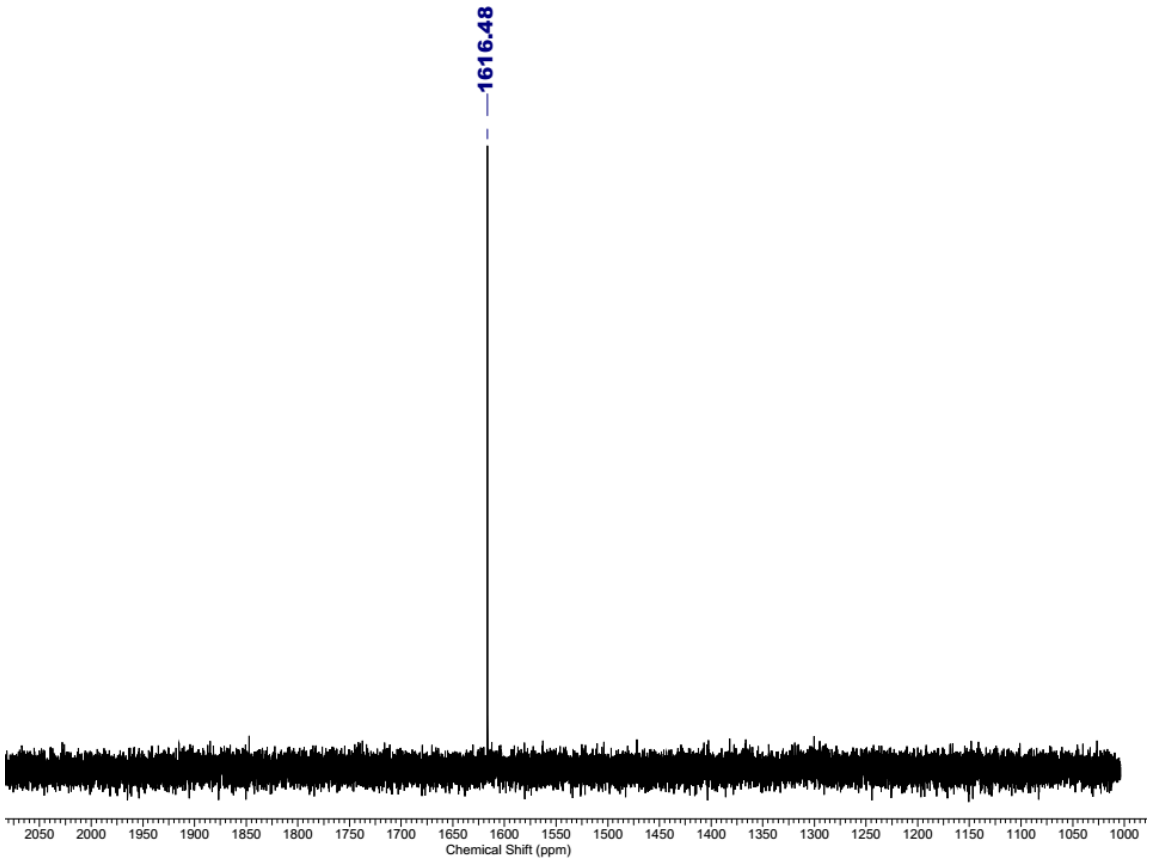

Fig. S9. ^{125}Te NMR spectrum of [Te(Cat^{36})$_2$(DAB^{Mes,H})]$_\infty$ (**6**) (CH_2Cl_2, 298K).

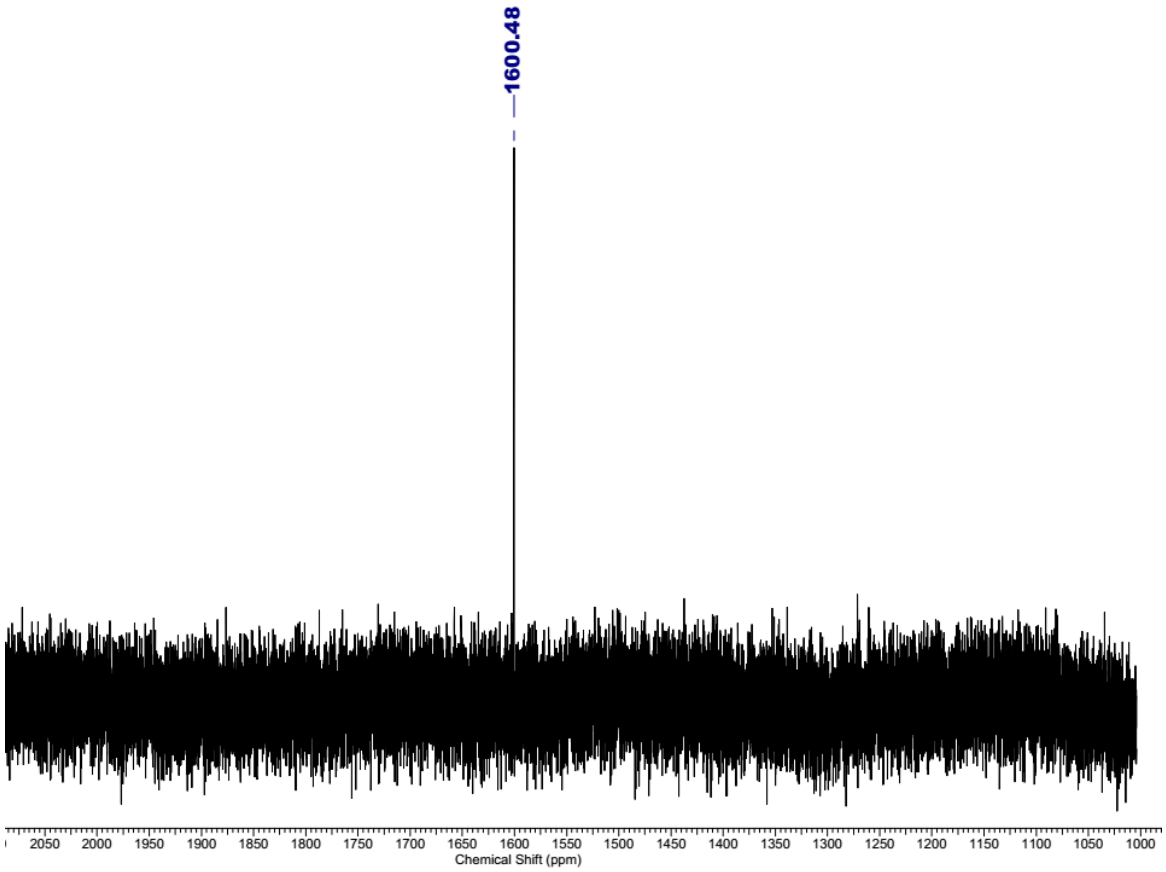

Fig. S10. ^{125}Te NMR spectrum of [{Te(Cat^{36})$_2$}$_2$(bpm)] (**7**) (CH_2Cl_2, 298K).

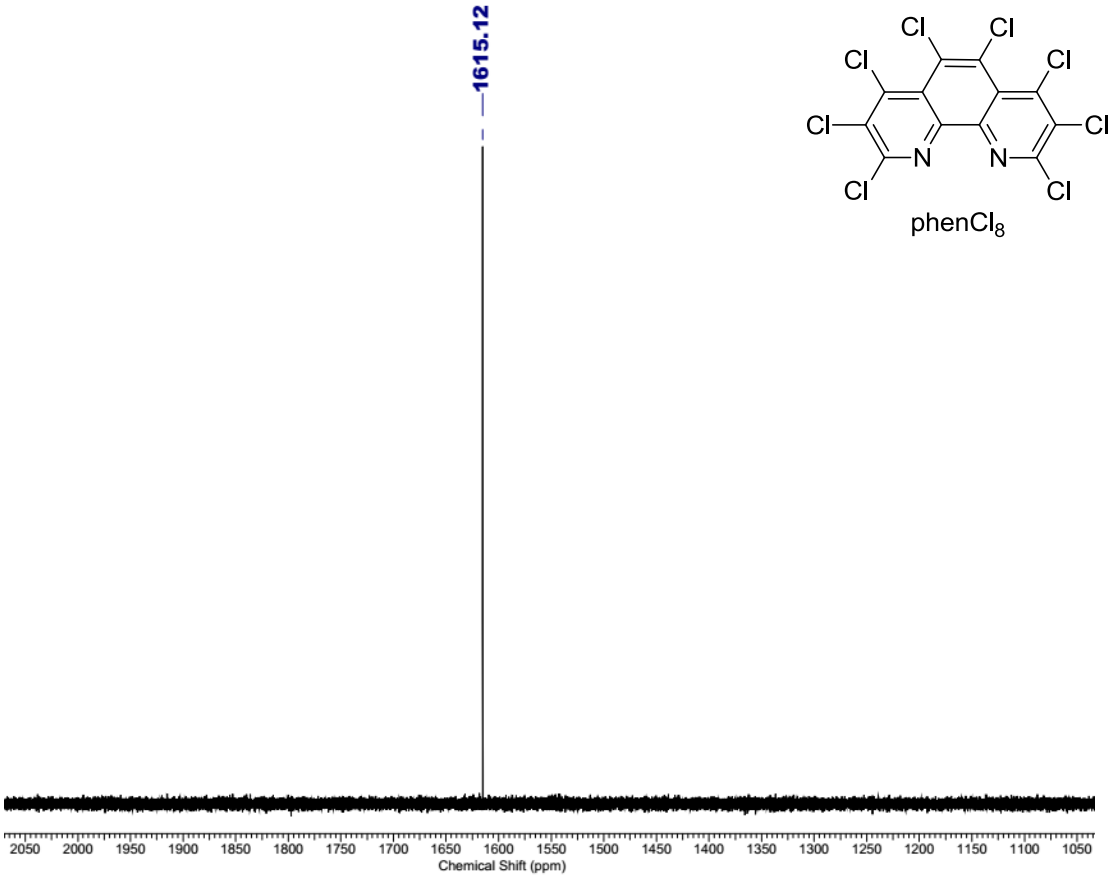

Fig. S11. ^{125}Te NMR spectrum of Te(Cat^{36})$_2$ with phenCl$_8$ (1.1 eq.) added (CH_2Cl_2, 298K).

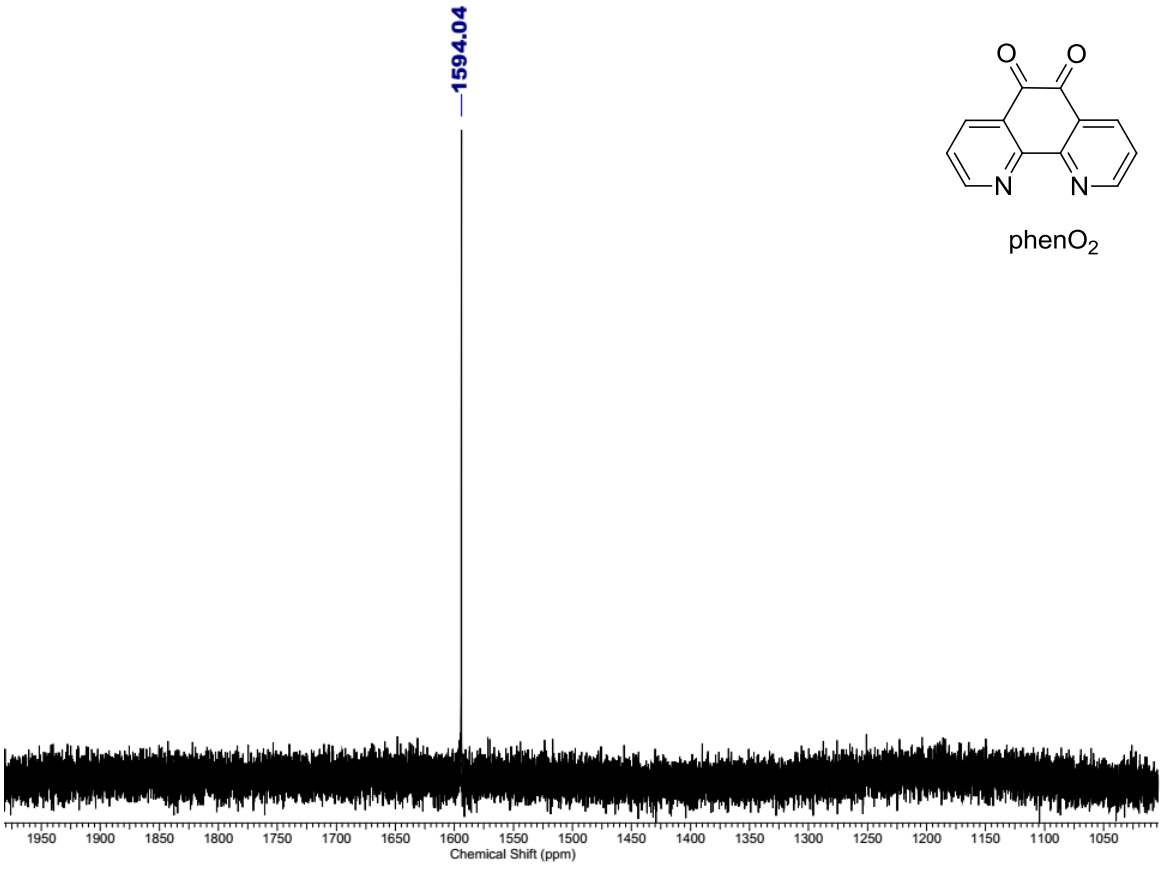

Fig. S12. ^{125}Te NMR spectrum of Te(Cat^{36})$_2$ with phenO$_2$ (1.1 eq.) added (CH_2Cl_2, 298K).

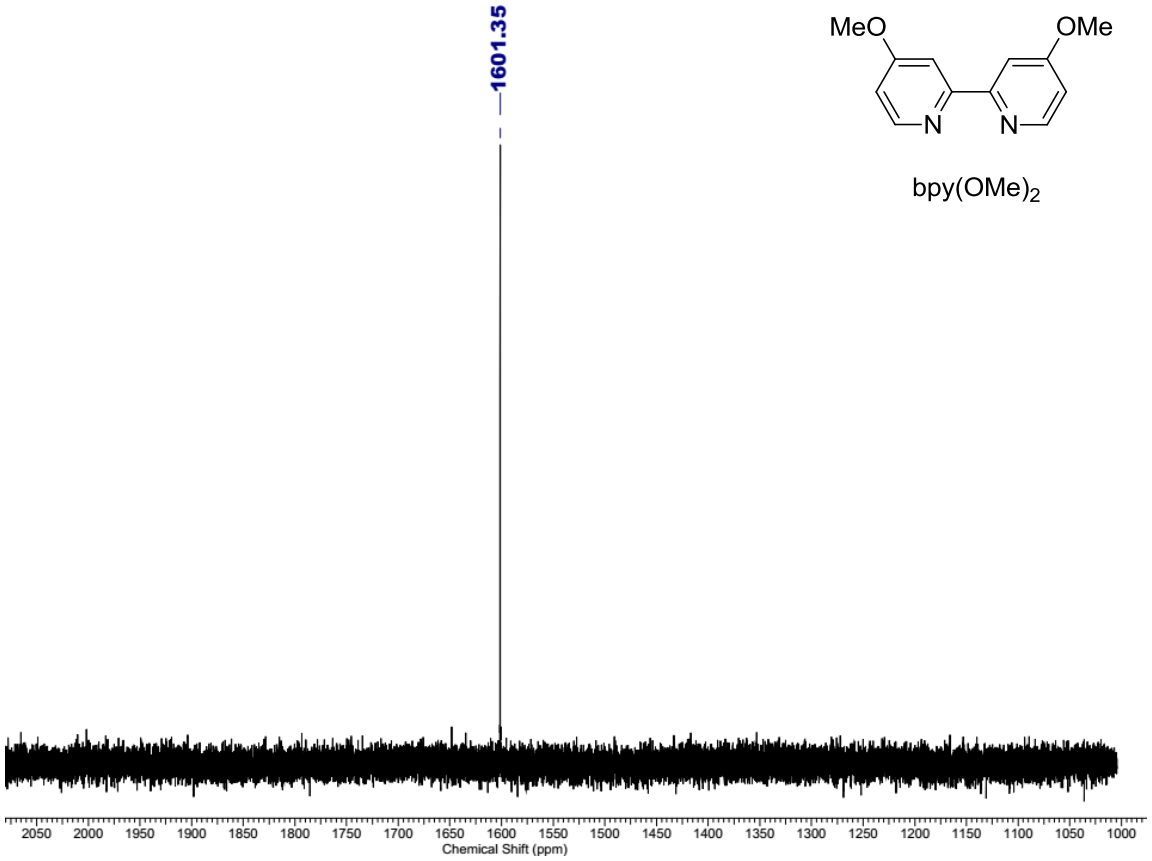

Fig. S13. ^{125}Te NMR spectrum of Te(Cat^{36})$_2$ with bpy(OMe)$_2$ (1.1 eq.) added (CH_2Cl_2, 298K).

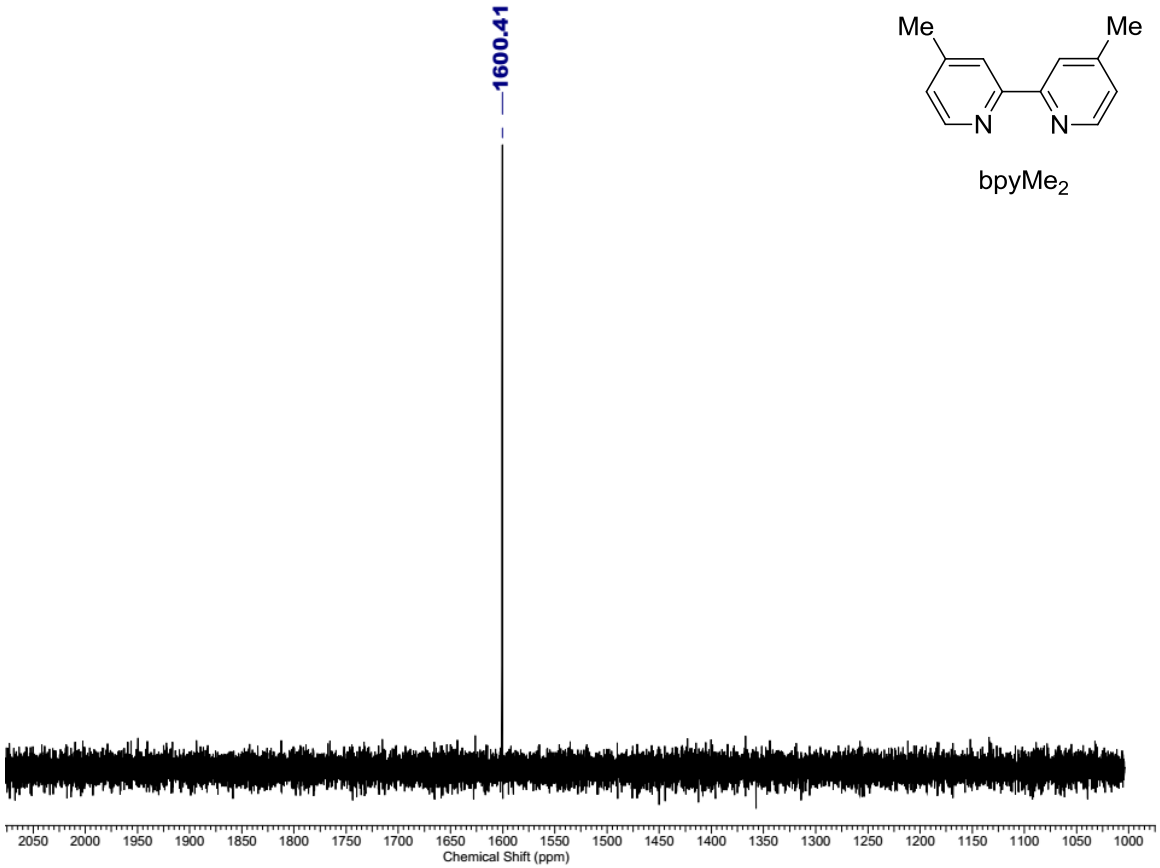

Fig. S14. ^{125}Te NMR spectrum of Te(Cat^{36})$_2$ with bpyMe$_2$ (1.1 eq.) added (CH_2Cl_2, 298K).

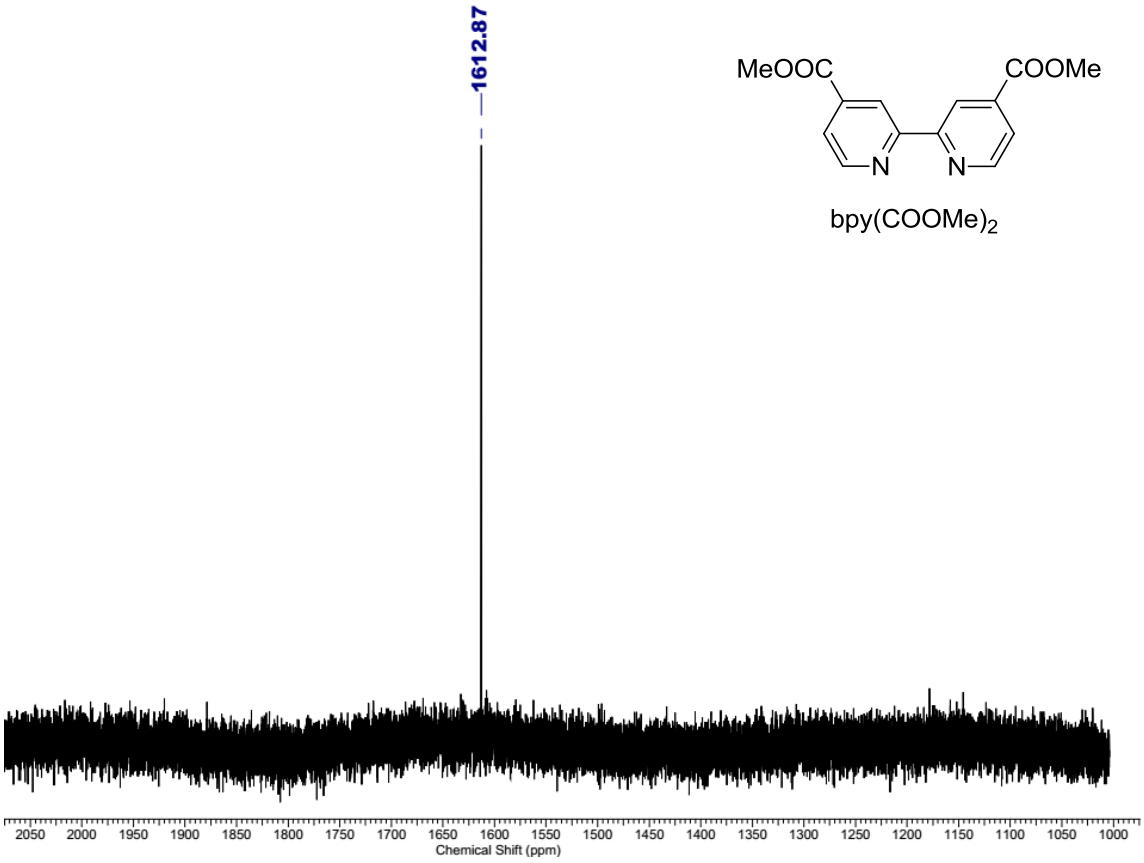

Fig. S15. ^{125}Te NMR spectrum of Te(Cat^{36})$_2$ with bpy(COOMe)$_2$ (1.1 eq.) added (CH_2Cl_2, 298K).

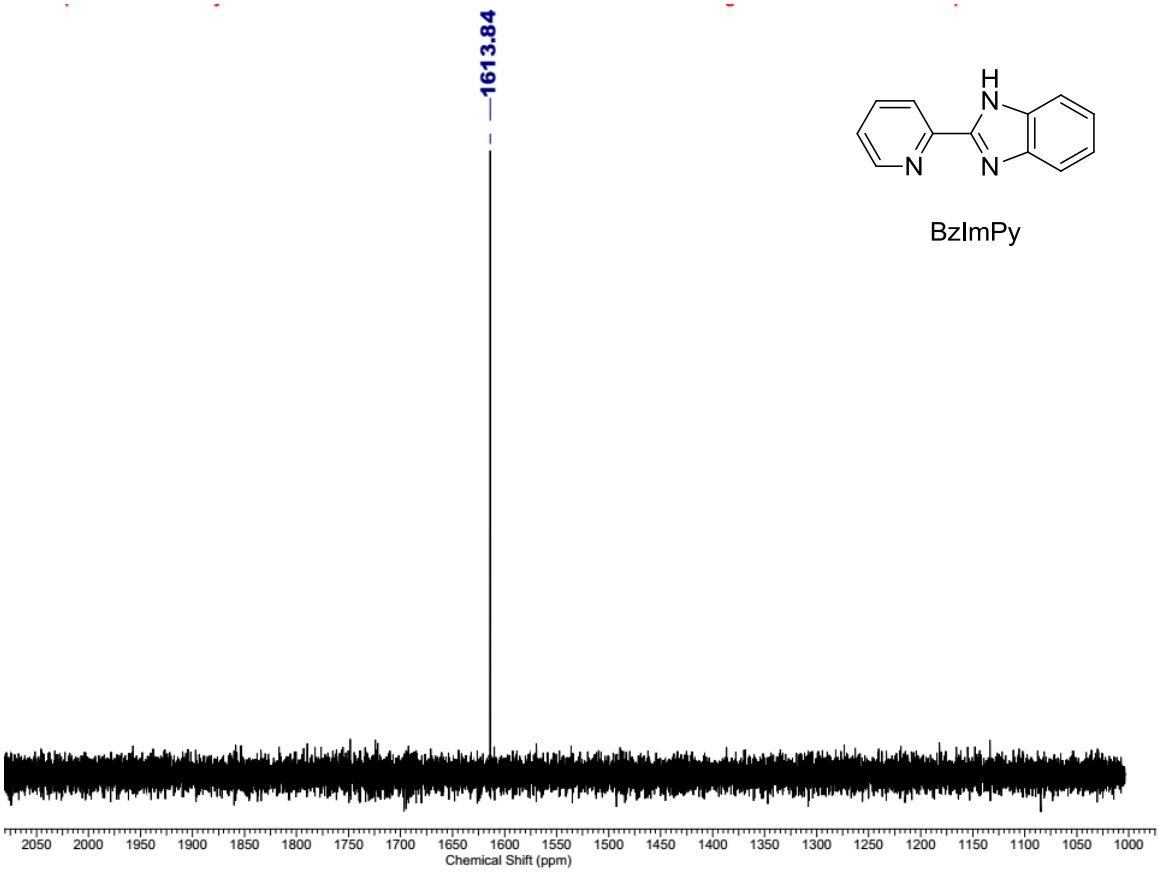

Fig. S16. ^{125}Te NMR spectrum of Te(Cat^{36})$_2$ with BzImPy (1.1 eq.) added (CH_2Cl_2, 298K).

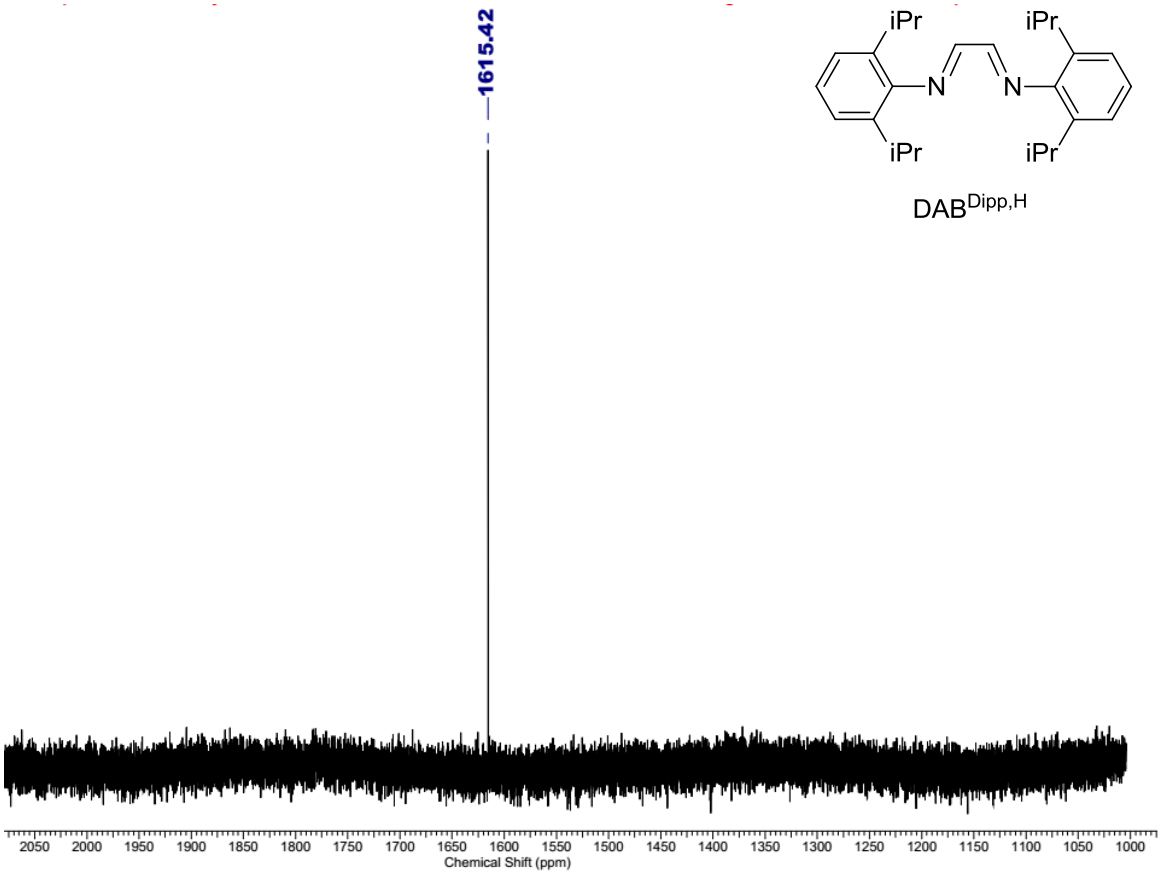

Fig. S17. ^{125}Te NMR spectrum of Te(Cat^{36})$_2$ with DAB^{Dipp,H} (1.1 eq.) added (CH_2Cl_2, 298K).

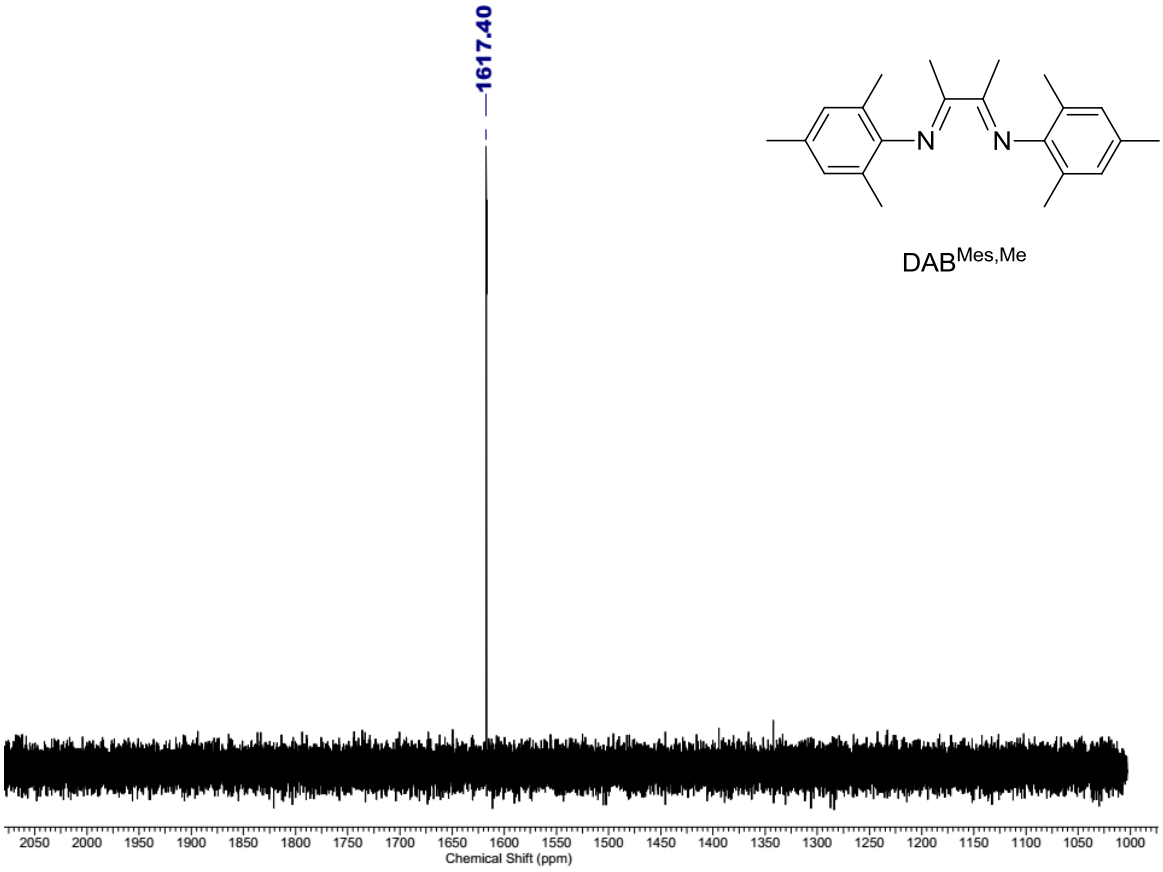

Fig. S18. ^{125}Te NMR spectrum of Te(Cat^{36})$_2$ with DAB^{Mes,Me} (1.1 eq.) added (CH_2Cl_2, 298K).

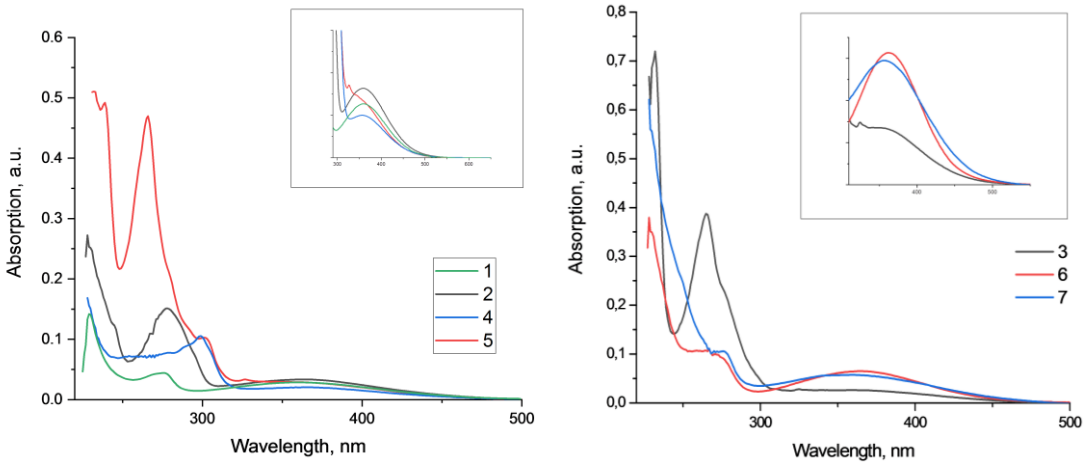

Fig. S19. UV-vis spectra of complexes **1–7** in CH_2Cl_2 solution.

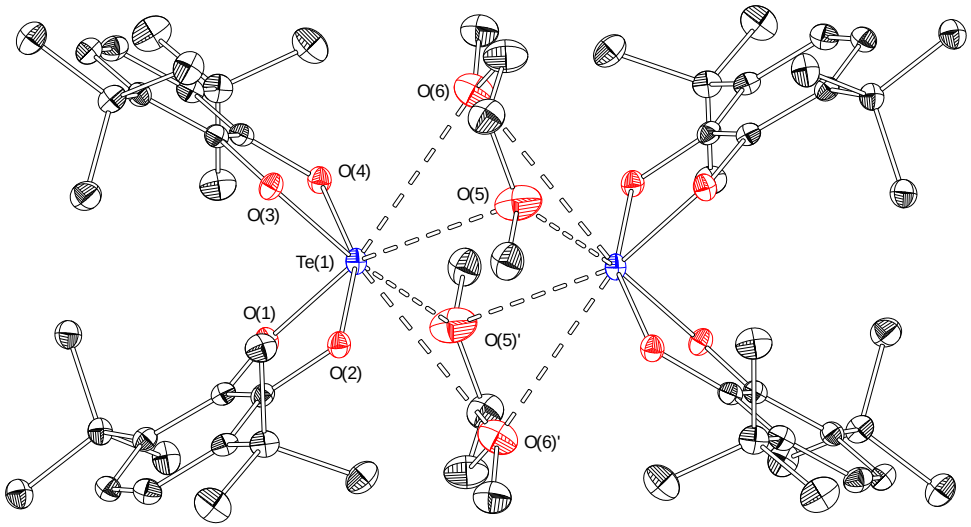

Fig. S20. Molecular structure of $[Te(Cat^{36})_2(dme)]_2$ (**8**) (dme – 1,2-dimethoxyetane). Thermal ellipsoids are given at the 30% probability level. Hydrogen atoms are omitted for clarity. Selected Te···O distances (Å): Te1···O5 3.002(2), Te1···O6 3.392(2), Te1···O6' 3.114(2), Te1···O5' 3.554(3) [1].

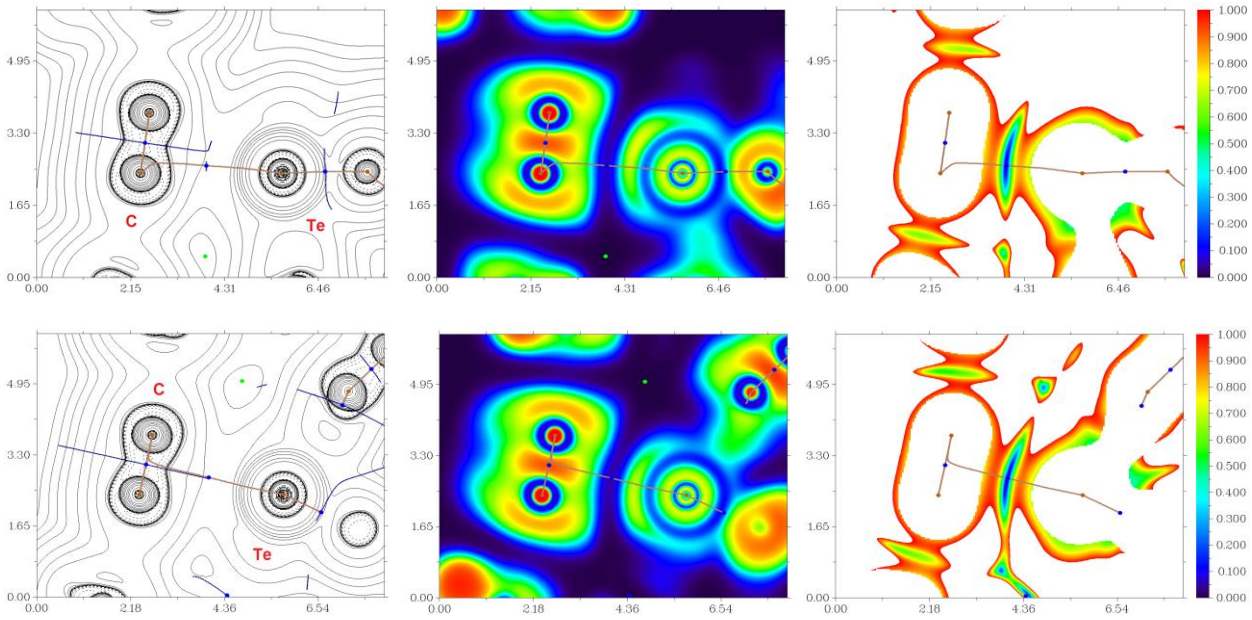

Fig. S21. Contour line diagram of the Laplacian of electron density distribution $\nabla^2\rho(\mathbf{r})$, bond paths, and selected zero-flux surfaces (left panel), visualization of electron localization function (ELF, center panel) and reduced density gradient (RDG, right panel) analyses for intermolecular interactions Te···C in **1** (top: environment of Te1, bottom: environment of Te2). Bond critical points (3, –1) are shown in blue, nuclear critical points (3, –3) – in pale brown, cage critical points (3, +3) – in light green, bond paths are shown as pale brown lines, length units – Å, and the color scale for the ELF and RDG maps is presented in a.u.

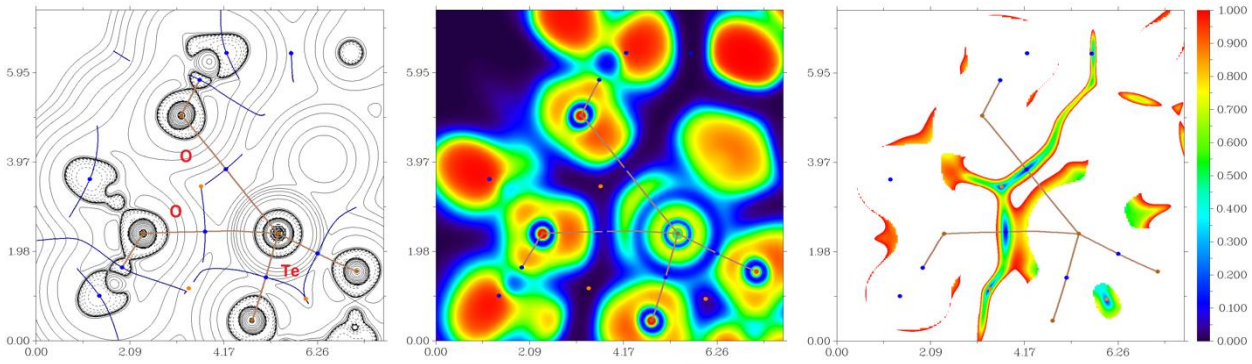

Fig. S22. Contour line diagram of the Laplacian of electron density distribution $\nabla^2\rho(\mathbf{r})$, bond paths, and selected zero-flux surfaces (left panel), visualization of electron localization function (ELF, center panel) and reduced density gradient (RDG, right panel) analyses for intermolecular interactions Te···O in **8**. Bond critical points (3, –1) are shown in blue, nuclear critical points (3, –3) – in pale brown, ring critical points (3, +1) – in orange, bond paths are shown as pale brown lines, length units – Å, and the color scale for the ELF and RDG maps is presented in a.u.

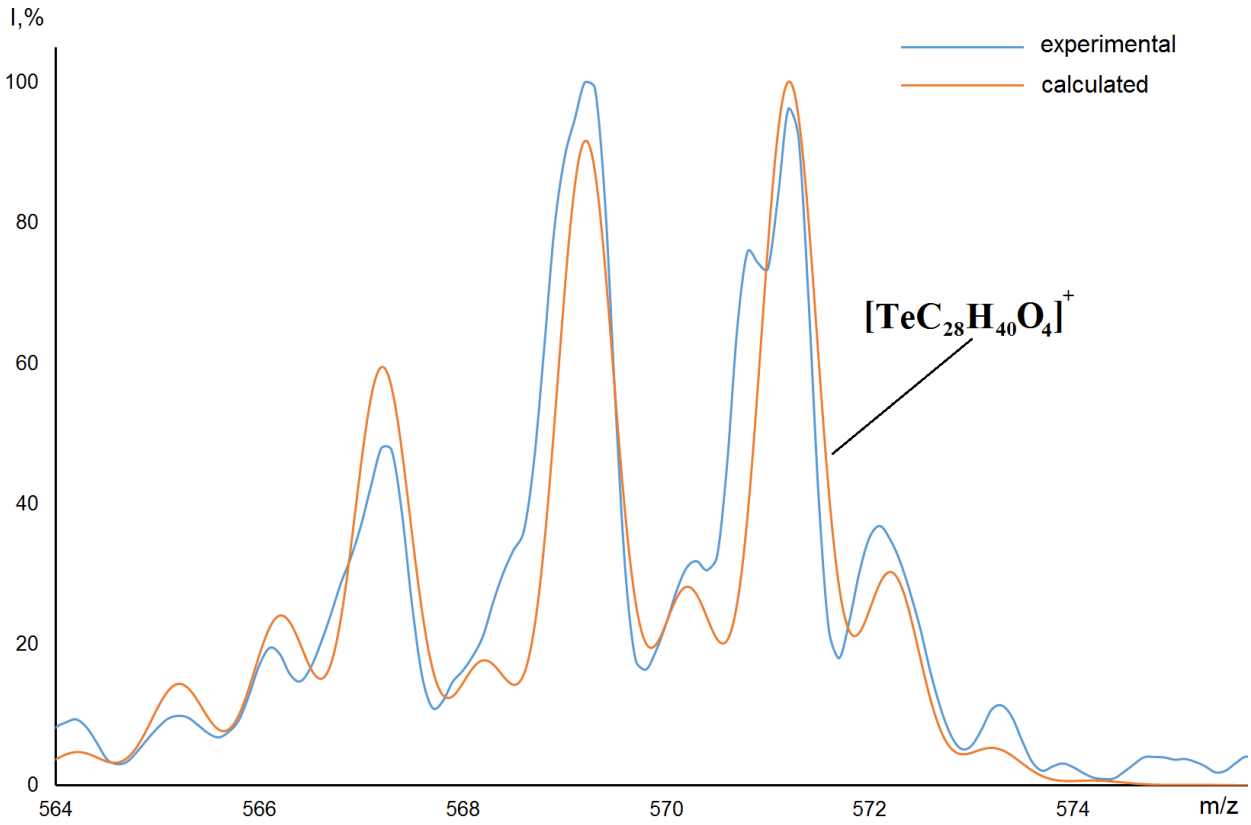

Fig. S23. (+)-ES-mass spectrum of Te(Cat^{36})$_2$ (**1**).

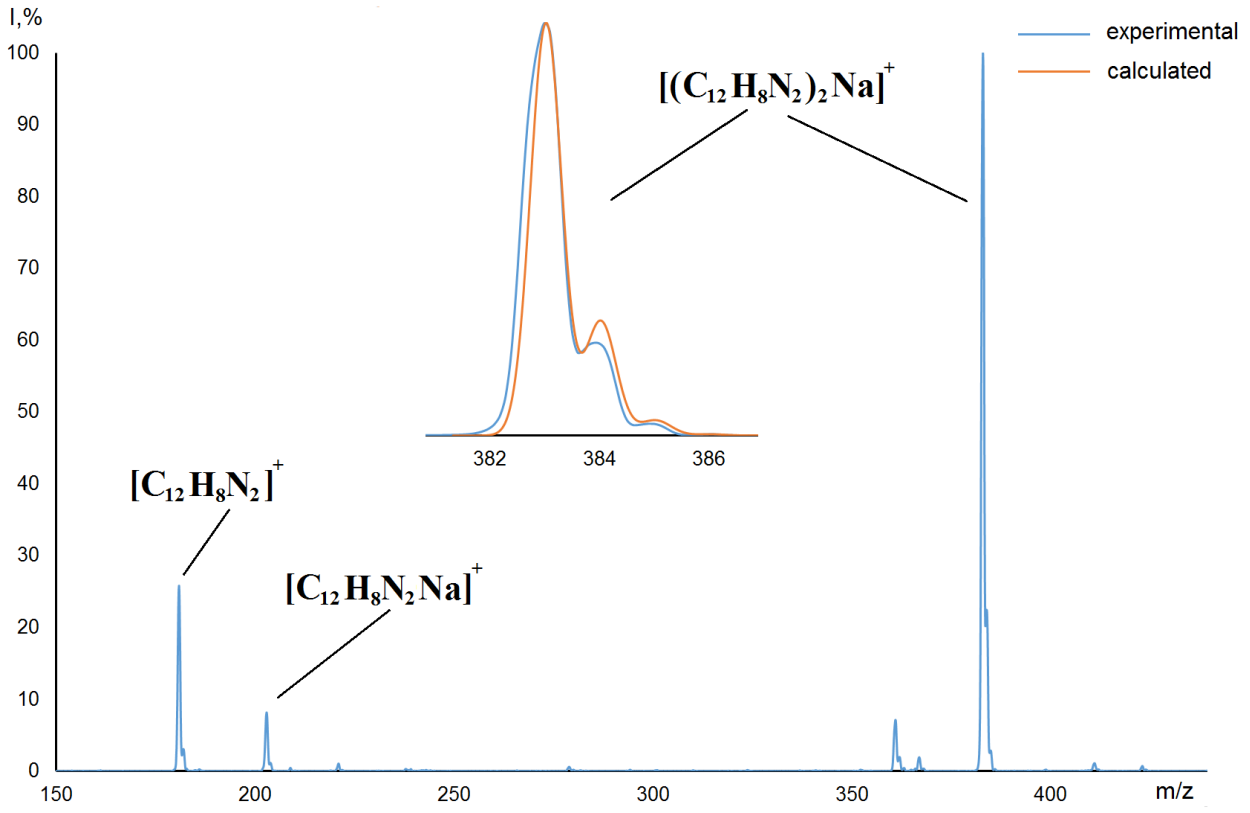

Fig. S24. (+)-ES-mass spectrum of [Te(Cat^{36})$_2$(phen)]$_2$ (**3**).

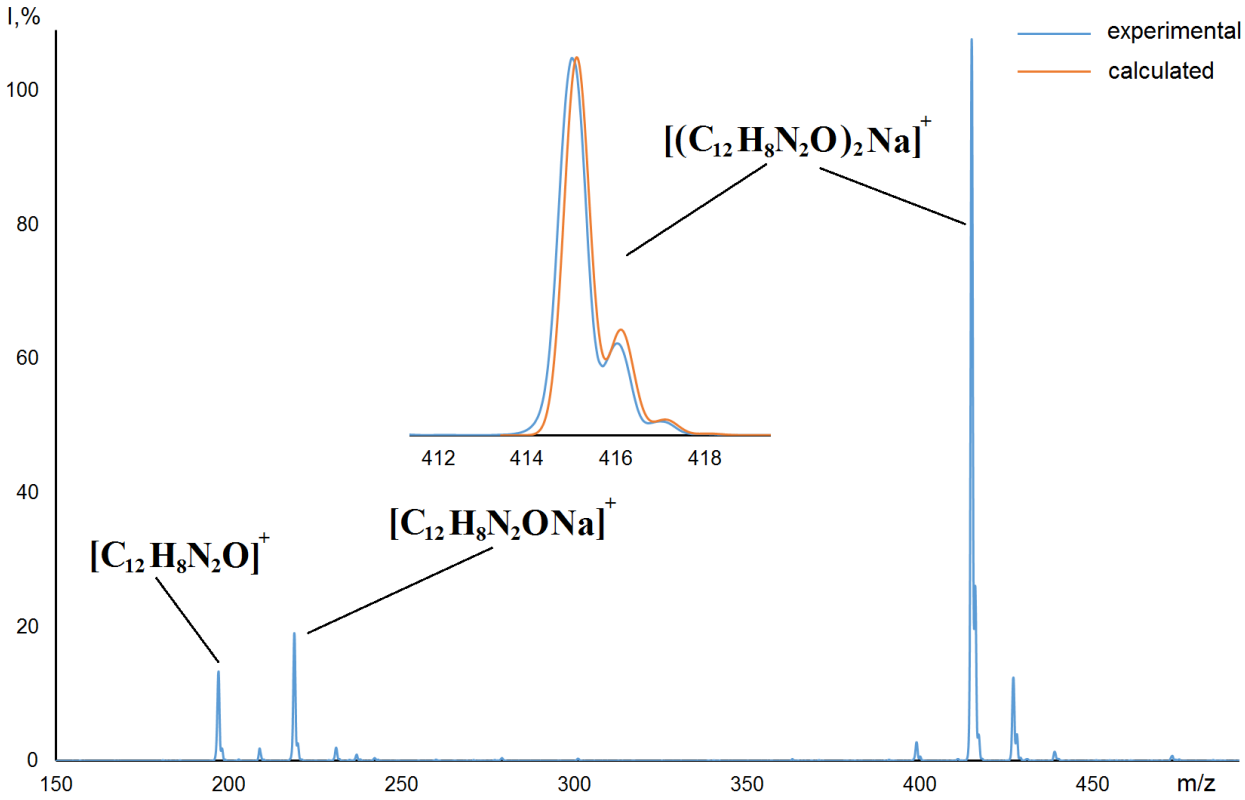

Fig. S25. (+)-ES-mass spectrum of $[Te(Cat^{36})_2(phenO)]_2$ (**4**).

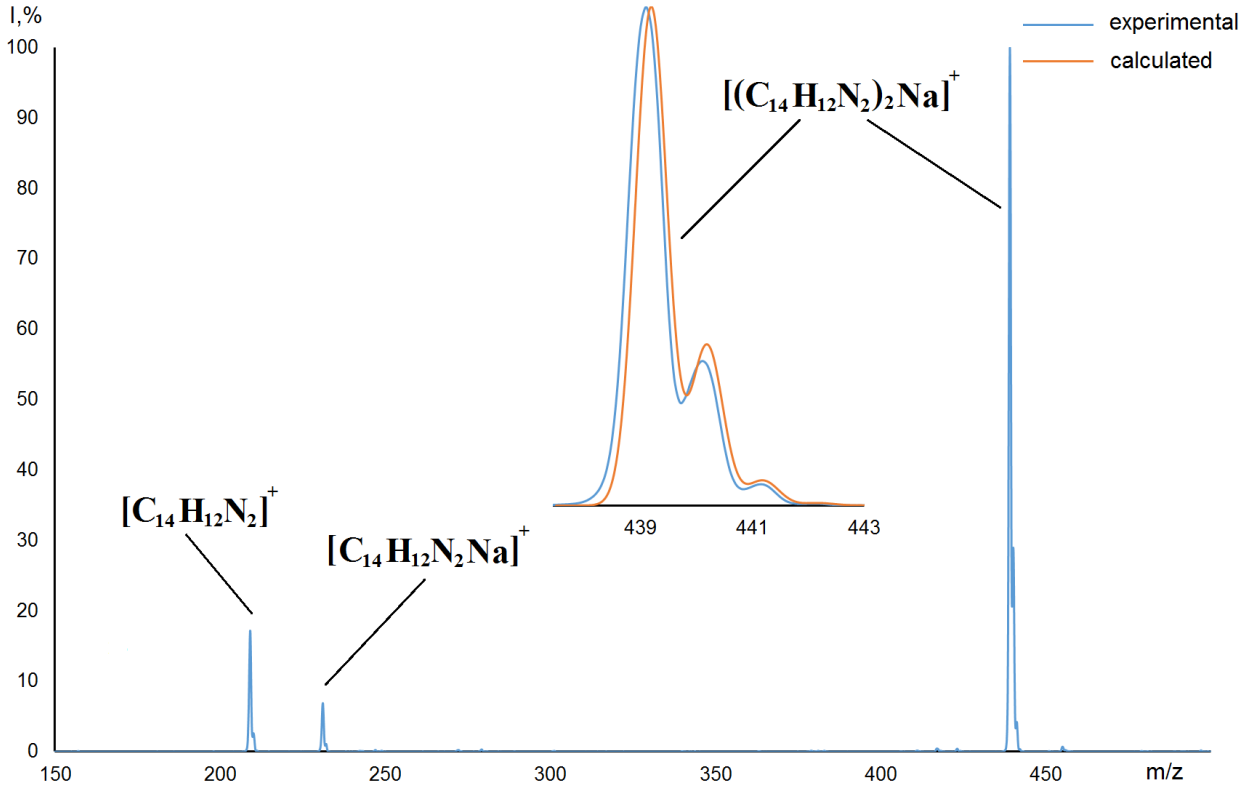

Fig. S26. (+)-ES-mass spectrum of $[Te(Cat^{36})_2(phenMe_2)]_2$ (**5**).

References

1. Petrov, P. A. Adducts of Sterically Hindered Tellurium Catecholate with Ethers. *Russ. J. Coord. Chem.*, **2023**, *49*, 357–362. doi: 10.1134/S1070328423600262